JOM, Vol. 76, No. 5, 2024
https://doi.org/10.1007/s11837-024-06485-7

Comparative Analysis and Error Assessment of Nanoindentation Evaluation Techniques for Nafion™117

VELISLAVA YONKOVA ,[1,5] NIKOLAI UTSCH ,[2] JULIAN BOROWEC ,[3,4] RÜDIGER-A. EICHEL ,[3,4] FLORIAN HAUSEN ,[3,4] FABIAN SCHEEPERS ,[2] STEFFEN BRINCKMANN,[1,6] and RUTH SCHWAIGER[1]

1.—Microstructure and Properties of Materials (IEK-2), Forschungszentrum Juelich GmbH, 52425 Juelich, Germany. 2.—Electrochemical Process Engineering (IEK-14), Forschungszentrum Juelich GmbH, 52425 Juelich, Germany. 3.—Fundamental Electrochemistry (IEK-9), Forschungszentrum Juelich GmbH, 52425 Juelich, Germany. 4.—Institute of Physical Chemistry, RWTH Aachen University, 52074 Aachen, Germany. 5.—e-mail: v.yonkova@fz-juelich.de. 6.—e-mail: s.brinckmann@fz-juelich.de

Advances in the application of polymers for electrochemical cells require an understanding of their viscous deformation mechanisms and their interaction with moisture. Nanoindentation offers a localized, microscale testing alternative to traditional tensile testing. However, the viscoelastic nature of the polymers, combined with their increased compliance, presents challenges in the analysis of nanoindentation results. In addition, the dependence on moisture results in significant scatter and low repeatability. This study combines nanoindentation and tensile testing as a verification method and compares different correction protocols for static nanoindentation to investigate the mechanical behavior of polymer electrolyte membranes. Comparisons of different indentation devices, analysis methods, and indentation protocols show a significant overestimation of Young's modulus using the classical Oliver–Pharr method compared to values determined from tensile tests. Nanoindentation at different humidity levels revealed different mechanisms leading to a decrease in Young's modulus and hardness with increasing humidity.

INTRODUCTION

Increasing renewable energy efficiency and its competitiveness to conventional fossil fuels has become crucial around the world. The energy crisis in Europe in 2022 was the latest example of the importance of renewable energy. Hydrogen technologies offer an appealing prospect for the in-depth decarbonization of global energy systems.[1]

Polymer electrolyte membrane fuel cells (PEMFC) and water electrolyzers use a polymeric proton-conducting material as an electrolyte. A typical membrane on the market is Nafion™ 117, which—as for all polymers—exhibits viscoelastic properties, i.e., it has a time-dependent mechanical response. Understanding the mechanical properties and deformation mechanisms of soft and compliant polymers like Nafion is therefore an integral part of the PEMFC performance investigation. For example, stress relaxation partially controls the water uptake, interfacial mass transport, diffusion, and polymer swelling of PEMFCs. On the one hand, polymer swelling due to water absorption and the clamping pressure leads to membrane creep, which can result in the separation of the electrodes from the membrane, i.e., delamination.[2,3] On the other hand, stresses in the PEMFC caused by clamping the membrane, or by changing its levels of hydration during operation, result in thinning spots, which may lead to the development of pinholes or contact between membrane and electrode.[4] These pinholes have also been linked to the swelling and thinning.[5,6]

(Received November 13, 2023; accepted February 23, 2024; published online April 1, 2024)

Tensile testing is the traditional macroscale tool for characterizing the mechanical behavior of polymers, including the viscoelastic properties as well as the behavior beyond the yield point.[2,7,8] At the microscale, nanoindentation provides Young's modulus and hardness; thus, the combination of these two methods seems promising to establish correlations between the macroscopic- and microstructure-related properties not only for PEMs but also for other compliant polymers.

Understanding the micromechanical deformation mechanisms of Nafion through nanoindentation could provide valuable information about the pinhole formation and other microscopic structural changes within the membranes. However, there are only a limited number of studies on nanoindentation of Nafion. Xia et al.[9] investigated the influence of temperature on Nafion using nanoindentation, but did not find a specific correlation with temperature. The loading conditions were shown to affect the apparent mechanical behavior. A faster load/unload rate, longer dwell time, and low maximum load helped to mitigate the creep effect in nanoindentation.[10] Zhang et al.[11] investigated the creep properties by nanoindentation and modeling, and observed a significant increase in creep displacement above 70°C due to the glass transition. In addition, using a dimensionless parameter, it was shown that the load could have a greater influence on creep than temperature.[11] The viscous properties of polymers pose a challenge to the nanoindentation method by introducing artifacts.[12,13] Nanoindentation measurements of polymers generally overestimate the Young's modulus in comparison to tensile tests.[14–16] Some authors[17,18] have proposed to correct the nanoindentation analysis approach for polymers by various modifications, such as increasing the holding time at the maximum load, faster strain rates, or analyzing only part of the unloading curve. These methods have never resulted in a generally accepted test and analysis protocol, and the observations regarding the mechanisms remain ambiguous.

This study aims to improve nanoindentation analysis for compliant polymers, such as Nafion. We examined the difficulties and intricacies of mechanical measurements of Nafion at both the micro- and macroscale using different nanoindentation protocols, analysis methods, and instruments. We studied their applicability with respect to reproducibility and accuracy, which will contribute to our understanding of polymer deformation and provide guidelines for investigating compliant polymers.

SAMPLES AND METHODS

Samples

Four Nafion117 membranes, treated with different solvent mixtures to simulate the coating process and to investigate whether the alcohol–water mixture affects the membrane stability in the absence of a metal catalyst, and one Nafion NR212 membrane with a different thickness compared to Nafion117, were prepared (Table I) and tested using tensile testing and nanoindentation. The solvent mixture for the cathode (K+) had a 1:2 ratio of n-propanol/water, while the solvent mixture for the anode (A−) had a 2:1 ratio for the same compounds. The membrane was placed on the heated vacuum plate of the ultrasonic coating system (ExactaCoat; Sono-Tek) before spraying the solvent mixture onto Nafion117. The temperature was set to 80°C for (K+) and 90°C for (A−), and the spray flow rates were 0.3 mL/min for (K+) and 0.2 mL/min for (A−). These conditions simulate typical spray parameters.[19] The membranes changed color and appeared yellow after treatment under certain conditions. To eliminate the discoloration, the Nafion117 membranes were soaked in deionized water after the spraying process. These samples are labeled with H_2O in Table I. After soaking the membranes, they were dried in ambient environment.

Tensile Experiments

The tensile samples were tested using a universal testing machine (Instron 4400; Instron, Darmstadt, Germany) equipped with a 5 kN load cell (Doli Elektronik, Munich, Germany). The samples were deformed using wedge grips, and the strain was determined based on the cross-head displacement, because the compliance of the frame is insignificant compared to the compliance of the polymer samples. The time-dependent force and displacements were converted into engineering stress and strain values, respectively, given the initial gauge dimensions of each sample measured. Figure 2 shows a typical stress–strain curve.

The force and displacement signals, and consequently stress and strain, exhibit considerable vibrations and inherent noise over time, which requires smoothing prior to analysis. The filtering stability was evaluated by the gradient δ:

$$\delta_i = \frac{\sigma_i - \sigma_{i-1}}{\epsilon_i - \epsilon_{i-1}} \quad (1)$$

where σ_i and ϵ_i represent the stress and strain values, respectively, in two adjacent time increments. The main objective of the filtering process is to preserve the gradient δ of approximately 20 (as illustrated in Fig. 1b), to ensure that a comparison between different measurement parameters is not affected by any distortions or phase shifts in the passband. Therefore, we retained the original data while minimizing any potential signal alterations and noise.

The scipy.signal package was used (scipy v.1.7.1) to apply the Butterworth and median filters.[20] First, we applied a low-pass Butterworth filter with an adjusted cut-off frequency. The cut-off frequency depends on the experimental parameters, such as the displacement rate. The corresponding cut-off

Table I. The five membranes tested in this work and the applied treatment on each of them, where "✔" is present and "none" is not present

Membrane	Label	Cathode	Anode	Hydration	Thickness (μm)
Nafion 117	Untreated	None	None	None	178
Nafion 117	K+/H_2O	✔	None	✔	178
Nafion 117	K+/A−/H_2O	✔	✔	✔	178
Nafion 117	K+/ A−	✔	✔	None	178
Nafion NR212	Untreated thin	None	None	None	51

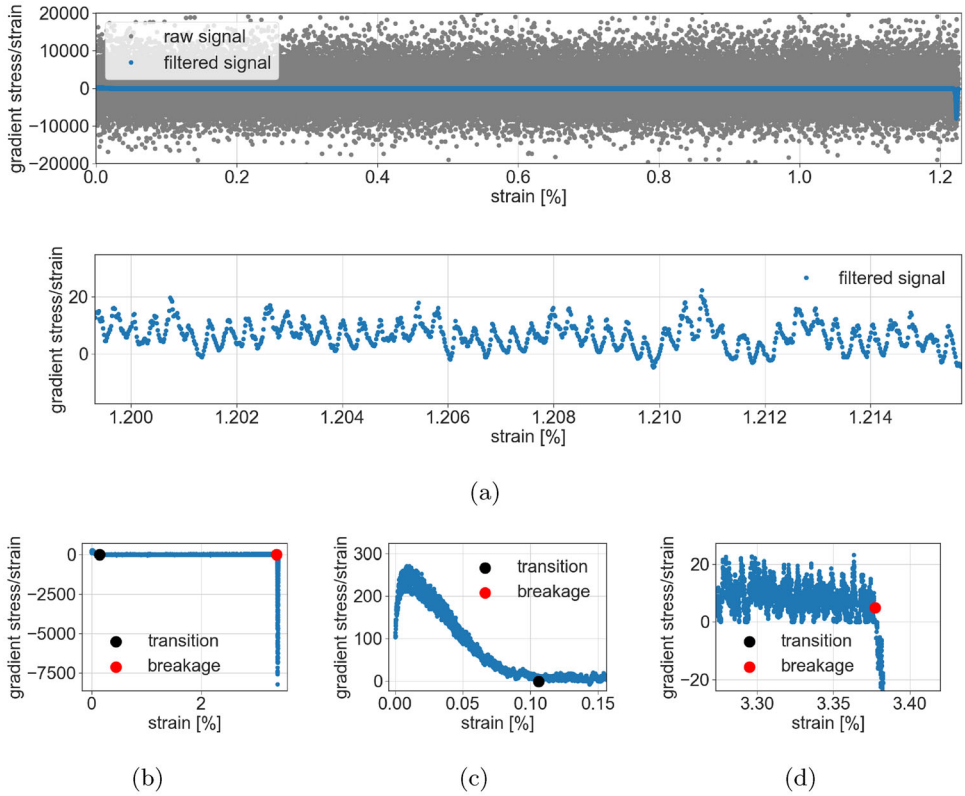

Fig. 1. Analysis of the stress–strain gradient δ (untreated Nafion117, displacement rate 5 mm/min): (a) unfiltered and filtered signals such that $m \sim 20$ is maintained. A zoom of the final displacement data highlights the remaining signal noise; (b) filtered signal and transition point between the elastic and plastic regimes (black) and the breakage point (red); (c) magnified region of the gradient δ around the transition point, which marks the beginning of an almost constant δ; (d) magnified region of the gradient δ around the breakage point, which is the last point before the load drop (Color figure online).

frequencies of $\frac{1}{150}\,s^{-1}$, $\frac{1}{15}\,s^{-1}$, and $\frac{1}{1.5}\,s^{-1}$ were used for displacement rates of 5 mm/min, 50 mm/min, and 500 mm/min, respectively, corresponding to strain rates of 0.002 s^{-1}, 0.02 s^{-1}, and 0.2 s^{-1}. The strain rate in the tensile tests was determined as $\dot{\epsilon} = \frac{v(t)}{L_0}$, where L_0 is the initial sample length and $v(t)$ the crosshead speed. The thin Nafion NR212 membrane, and a displacement rate of 500 mm/min , produced the highest noise/signal ratio. To improve the signal, a median filter with a kernel size of 21 was applied. After smoothing the signal, specific curve segments and points were identified (Fig. 2) to quantify the scatter and evaluate the validity of the results:

1. Young's modulus, E was evaluated from a linear fit to the curve in the elastic regime:[21]

$$E = \frac{\sigma_{\text{elastic}}}{\epsilon_{\text{elastic}}} = \frac{F/A_0}{\Delta_L/L_0} \tag{2}$$

where σ_{elastic} and $\epsilon_{\text{elastic}}$ are the stress and strain in the elastic regime, respectively, F is the applied force, A_0 the initial cross-sectional area, L_0 the initial sample length, and Δ_L the crosshead displacement.

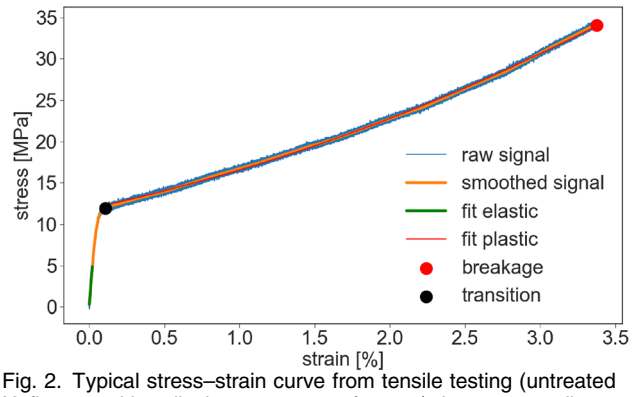

Fig. 2. Typical stress–strain curve from tensile testing (untreated Nafion117 with a displacement rate of 5 mm/min corresponding to a strain rate of 0.002 s^{-1}) and the applied processing steps. The unfiltered signal is in blue, the low-pass filtered signal in orange (Butterworth filter). The transition from elastic to plastic deformation is marked with a black cross; material failure is marked with a red cross. The linear part of the stress/strain curve, which is below 40% of the stress in the transition point, is used to determine the elastic slope (green line); the plastic regime is fitted by a second order polynomial (red line) to the stress–strain curve after the stress in the transition point (Color figure online).

2. The plastic deformation, κ, was determined as the slope in the plastic regime based on a second order polynomial fit:

$$\kappa = \frac{\sigma_{\text{plastic}}}{\epsilon_{\text{plastic}}} = \frac{F/A_0}{\Delta_L/L_0} \tag{3}$$

3. The transition point is the point at which elastic deformation ends and plastic deformation begins. To minimize the influence of signal noise in the elastic region of the curve, the transition point is defined as the 10th point after the gradient δ assumes a negative value for the first time (Fig. 1c).
4. The breakage point is defined as the last point with a positive gradient δ.

Young's modulus of a membrane is a measure of elasticity or stiffness of the material, indicating the maximum allowable mechanical deformation before the membrane undergoes irreversible deformation. A membrane deformed in the elastic regime can recover to its original state after unloading and remain stable during operation. However, if the deformation exceeds the transition point, the membrane will experience plastic deformation, resulting in permanent neck propagation and thinning, ultimately leading to failure at the breakage point.

Nanoindentation Experiments

To evaluate the effectiveness of the analysis methods, two different instruments were used: a Nano XP nanoindenter (MTS Systems, Eden Prairie, MN, USA) with a diamond Berkovich tip, and a Fischerscope H100 indenter (Helmut Fischer, Sindelfingen, Germany), with a diamond Vickers tip. The Fischerscope was placed inside a glove box under a protective Ar environment with minimal humidity ($\sim 0.1\%$). The untreated Nafion117 membrane was cut into 1 cm $\times$ 1 cm pieces and glued on a steel substrate with cyanoacrylate glue, ensuring that there was no air between the membrane and the substrate. The membranes had a surface roughness R_a of $\sim$ 18 nm as measured with an Olympus LEXT OLS4000 3D microscope.

We conducted an additional set of experiments on the untreated Nafion117 membrane using a Nano XP indenter and a Hysitron TI 980 triboindenter (Hysitron, now Bruker, Eden Prairie, MN, USA) with a Berkovich tip and a XSol humidity cell to measure the influence of relative humidity (RH) in the sample during the nanoindentation experiments. With the Hysitron setup, we were able to directly control the RH. The membrane sample was tested in both ambient conditions (RH 30%) and elevated humidity (RH 90%) without any change to its initial dry state. The measurements were conducted at a temperature of 30°C. Prior to each measurement, a settling time of 1 h was maintained to achieve humidity equilibrium between the environment and the sample. According to Bauer et al.,[22] Nafion reaches humidity equilibrium in 25 min. For comparison, dry and wet membranes were tested under ambient conditions using the Nano XP to mimic changes of RH.

The dry sample, i.e., the control sample for testing the effect of moisture, was prepared by keeping the sample in the glove box for 5 days, resulting in a water content of $\sim 0\%$, which was determined by gravimetry. The wet sample was in water for 3 days and excess water droplets were removed. The water content was determined gravimetrically as $20.1 \pm 1.6\%$ based on three measurements of three samples, which is in good agreement with literature values.[23] A completely dried sample (with 0% water content) underwent a rapid rehydration process in the indenter chamber within a few minutes. Despite rehydration, the water content did not exceed 7% under ambient conditions when the laboratory humidity varied between 20 and 40% (measured with a portable USB temperature and relative humidity data logger (EL-USB-2-LCD; EasyLog, UK) during summer and winter.

The indentation experiments performed with the Nano XP and Fischerscope were load-controlled, and the Nafion117 membranes were loaded at two different load rates. In the Nano XP, constant load rates of 0.15 mN/s and 1.5 mN/s were applied, to a maximum load of 15 mN, then the maximum load was held constant for 15 s and 60 s, respectively, to allow for a variation of the viscoelastic response during unloading. In the Fischerscope, the load was applied according to $d\sqrt{p}/d\,t$ to the same maximum load. The load was applied in 100 s and 10 s followed by a hold segment of 15 s and 60 s, respectively. The unloading time was equal to the loading time for all the experiments. For comparison with the tensile

Table II. Summary of the nanoindentation instruments used on Nafion117 in this study, analysis methods,[14,17,18] and settings (shown as maximum load/loading time/holding time)

Test	Purpose	Instruments	Settings	Analysis
1	Comparison of analysis methods	Nano XP; Fischerscope	15 mN/100 s/15 s; 15 mN/10 s/60 s	Ocliver–Pharr,[17] Ngan,[25] Mokhtari[14]
2	Investigation of humidity influence	Nano XP Hysitron	15 mN/10 s/60 s 3 μm/10 s/60 s	Oliver–Pharr[17]

tests, the strain rate during the indentation experiments was estimated as $\dot{\varepsilon} = \frac{\dot{h}}{h} = \frac{1}{2}\frac{\dot{p}}{p}$ [24] considering maximum load and loading time. However, it needs to be noted that the strain rate was not constant during the indentation experiments. A drift correction was not applied because the thermal drift was below 1 nm/s; thus, the displacement variation due to thermal drift relative to the maximum displacements of 6 μm was negligible. The experiments performed with Hysitron were displacement-controlled, the maximum set displacement was 3 μm, the loading time was 10 s, and the hold time was 60 s. The unloading time was equal to the loading time. The nanoindentation experiments and instruments used are summarized in Table II.

Analysis of Nanoindentation Data

The viscoelastic nature of polymers renders the Oliver–Pharr method[17] unsuitable for their mechanical characterization.[26] Over the years, several corrections have been proposed to improve the Oliver–Pharr method for polymers, two of which will be evaluated in this study. We started the analysis of the indentation data by determining the stiffness, S, from the unloading portion of the load–displacement (P–h) curves using a power law fit with parameters B, h_f and m:

$$S = \frac{dP}{dh}|_{h=h_{max}} = B(h - h_f)^m|_{h=h_{max}} \quad (4)$$

Oliver and Pharr[17] established that the contact depth h_c can be evaluated from the depth for axisymmetric tips by using a geometric constant $\varepsilon = 0.75$:

$$h_c = h - \varepsilon\frac{P}{S} \quad (5)$$

The contact area A_c was then evaluated based on the contact depth as $A_c = 24.5h_c^2$. Since in this study indents 4–6 μm deep were analyzed, a perfect tip shape was assumed. The reduced modulus was determined using:

$$E_r = \frac{\sqrt{\pi}S}{2\sqrt{A_c}} \quad (6)$$

The hardness is $H = \frac{P_{max}}{A_c}$.

Finally, Young's modulus of the material was determined from $\frac{1}{E_r} = \frac{1-\nu^2}{E} + \frac{1-\nu_I^2}{E_i}$, assuming $\nu_I = 0.07$ and $E_i = 1140$ GPa for Poisson's ratio and Young's modulus of diamond, respectively, and $\nu = 0.49$ for Poisson's ratio of Nafion.[9]

Following the approach introduced by Mokhtari et al.,[14] we analyzed the unloading stiffness at different time increments along the loading curve instead of evaluating the stiffness only at 98% of P_{max}. Following this approach, good agreement of Young's modulus values of thermoplastic polymers determined by nanoindentation and tensile tests was reported,[14] while the Oliver–Pharr method overestimated Young's modulus by a factor of three. In the following, the incremental analysis of the unloading curve will be referred to as the Mokhtari-correction.

In addition, we analyzed our data following the approach introduced by Ngan et al.,[18,25] which is based on a correction of the apparent stiffness, S, and provides a corrected stiffness S_e:

$$\frac{1}{S_e} = \frac{1}{S} - \frac{\dot{h}_h}{\dot{P}_u} \quad (7)$$

where S is the apparent contact stiffness at the onset of unloading (Eq. 4), $\dot{h}_h$ is the displacement rate determined using the numpy gradient function[27] over the last half second prior to unloading, and $\dot{P}_u$ is the prescribed unloading rate. Young's modulus is then determined using S_e in Eq. 6. We will refer to this method as the Ngan-correction in the following.

RESULTS AND DISCUSSION

Tensile Experiments

Figure 3 shows the stress–strain curves for the membranes with different surface treatments (Table I) deformed at a displacement rate of 5 mm/min. The elastic segments of the deformation curves are compared for the five membranes (Fig. 3a), resulting in comparable Young's modulus values between 0.21 GPa and 0.23 GPa (Fig. 3b). The thin membrane, Nafion NR212, showed a larger spread in the curves and a larger standard deviation in the elastic modulus compared to the Nafion117 membranes because the machine vibrations have a

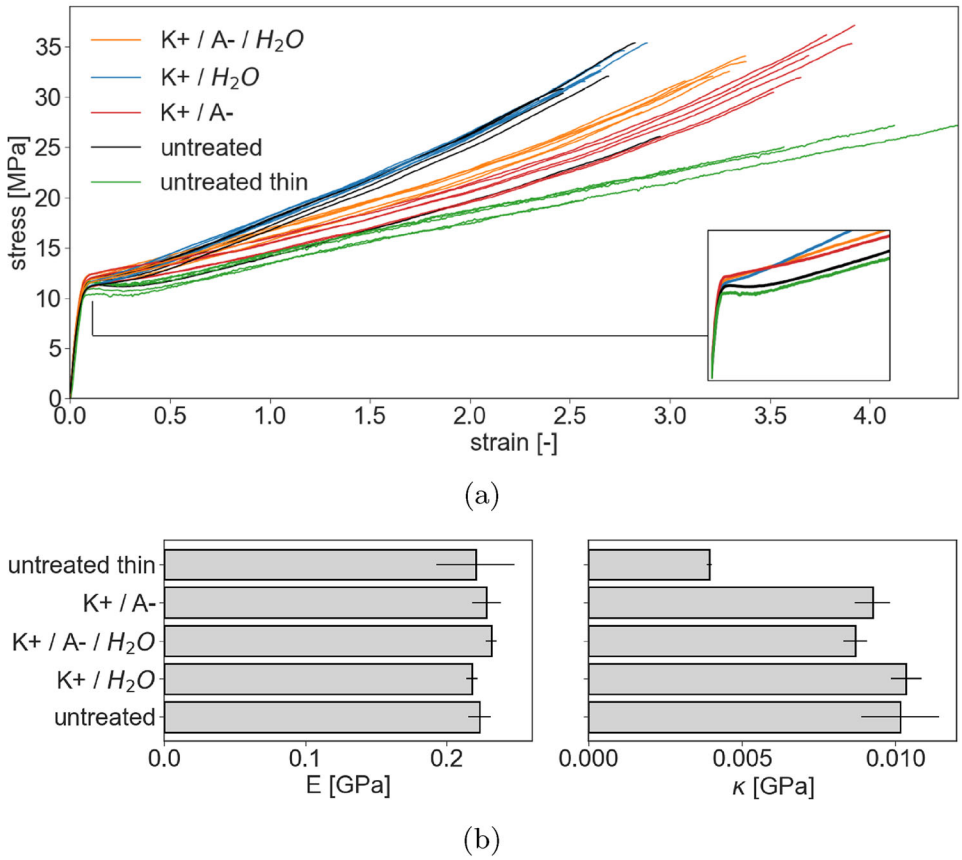

Fig. 3. (a) Stress–strain curves for membranes with different surface treatments and thickness deformed at a displacement rate of 5 mm/min (corresponding to a strain rate of 0.002 s^{-1}) and the determined mechanical properties at ambient conditions; inset the crease at the yield point. (b) Young's modulus, E, evaluated in the elastic regime (on the left) and slope κ evaluated in the plastic regime (right). Both slopes account for initial specimen geometry. Error bars correspond to the standard deviation of the mean value (of at least five measurements).

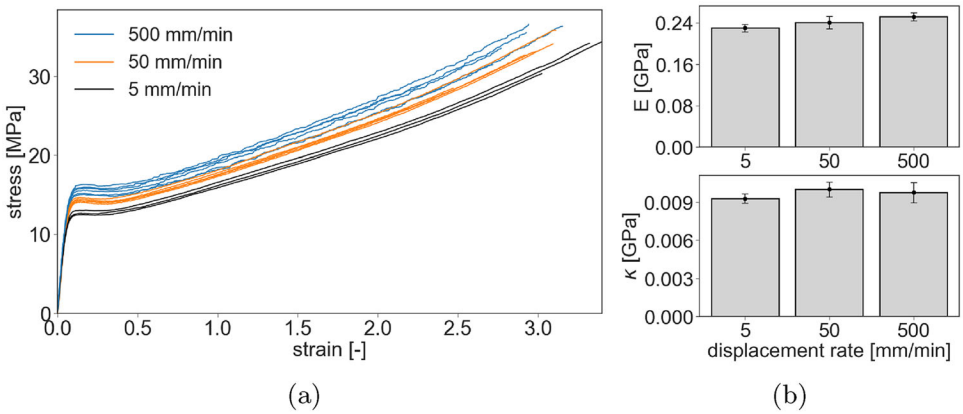

Fig. 4. Viscoelastic behavior of the untreated Nafion117 membrane and the mechanical properties determined: (a) stress–strain curves determined at different displacement rates, i.e., 5 (in black), 50 (in yellow) and 500 mm/min (in blue), corresponding to strain rates of 0.002 s^{-1}, 0.02 s^{-1}, and 0.2 s^{-1} respectively; (b) Young's modulus, E, and slope in the plastic deformation regime κ. Error bars represent the standard deviation of the mean value, derived from a minimum of three measurements (Color figure online).

greater effect on the thin membrane results than for the thicker Nafion117 membranes.

In our investigation, we note a distinct crease in the stress–strain curves of untreated membranes at the yield point (illustrated by the black and green curves in the inset of Fig. 3a). This crease occurring at the transition from elastic to plastic behavior is particularly pronounced in the thinner membrane, Nafion NR212. indicating the onset of necking and that the yield point was reached. The corresponding yield strength ranged between 10 MPa and 12 MPa. Subsequently, the necking phenomenon propagates and stabilizes, at which point homogeneous deformation was observed until rupture.[28,29] Notably, the introduction of (K+), (A−), or H_2O treatments eradicated the observed crease in stress–strain behavior, indicating more homogeneous deformation without necking instability in the tensile specimens subjected to surface treatments.

When comparing the membranes, notable differences in their tensile behavior become more pronounced beyond the yield point. The treated and untreated membranes exhibit distinct variations in the failure stress and failure strain, spanning from 200% to 400% for failure strain and 25–35 MPa for failure stress. These distinctions are further elucidated in the bar graph (Fig. 3b) on the right), depicting the slope of plastic deformation κ leading up to failure, which ranges from 0.04 GPa to 0.1 GPa.

The observed differences in mechanical properties between the membranes subjected to different surface treatments can be attributed to variations in the molecular alignment of polymer chains during the initiation and propagation of necking, which occurs during plastic deformation.[28] Surface roughness may introduce initial imperfections, potentially resulting in a more pronounced scatter of failure strain values. Additionally, environmental factors such as humidity, which could induce slight changes in membrane thickness[30] and temperature, may influence the observed differences in κ.

As expected, and shown in Fig. 4, the stress–strain curves, along with the slopes in the elastic and plastic deformation regimes, i.e., Young's modulus and κ, depend on the displacement rate.

Young's modulus exhibited a slight increase with higher displacement rates, as depicted in Fig. 4b. The yield strength, representing the stress at the yield point, increased with increasing displacement rate from 12 MPa for 5 mm/min to 16 MPa for 500 mm/min. However, due to the notable variability in failure strain (ranging from 240% and 340%) and failure stress (ranging from 29 MPa and 36 MPa), these parameters could not be correlated with the displacement rate. Despite this variability, the behavior in the plastic deformation regime, beyond the yield point, was very consistent for the tests conducted at different displacement rates. This consistent behavior was reflected in the similarity

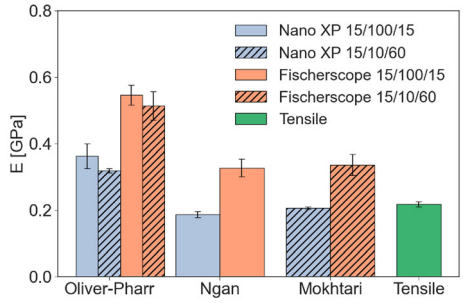

Fig. 6. Comparison of Young's modulus for untreated Nafion117 determined by different methods and instruments. The nanoindentation experiments used a maximum load of 15 mN, a loading time of 100 s , and a holding time of 15 s (strain rate: 0.005 s^{-1}) for the Ngan-correction and 15 mN, loading time of 10 s ,and a holding time of 60 s (strain rate: 0.05 s^{-1}) for the Mokhtari-correction. The values determined by the Oliver–Pharr method[17] were evaluated for both test conditions and the test conditions are shown in the legend as maximum load/loading time/holding time. The values determined by tensile testing are average values of tests conducted at the displacement rates of 5 mm/min, 50 mm/min, and 500 mm/min. Error bars correspond to the standard deviation of the mean value (of at least 5 measurements) (Color figure online).

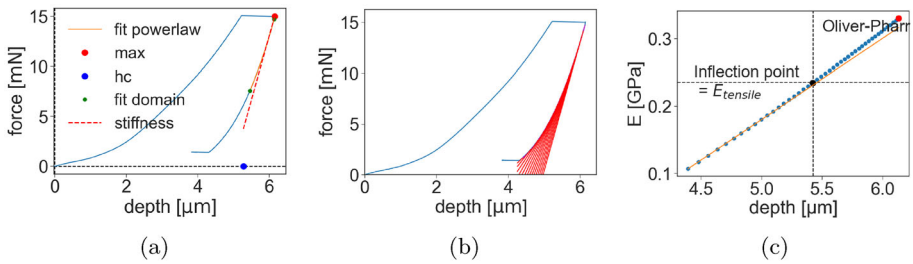

Fig. 5. Analysis of the load–displacement curve for untreated Nafion117, with a maximum load of 15 mN, a loading time of 10 s , and holding time of 60 s: (a) evaluation according to the Oliver–Pharr method[17] with the stiffness in red, evaluated at one point during unloading; (b) stiffness evaluated at different time increments during unloading according to the Mokhtari-correction;[14] (c) Young's modulus as a function of depth evaluated along the unloading curve according to the Mokhtari-correction in (b), showing an inflection point (Color figure online).

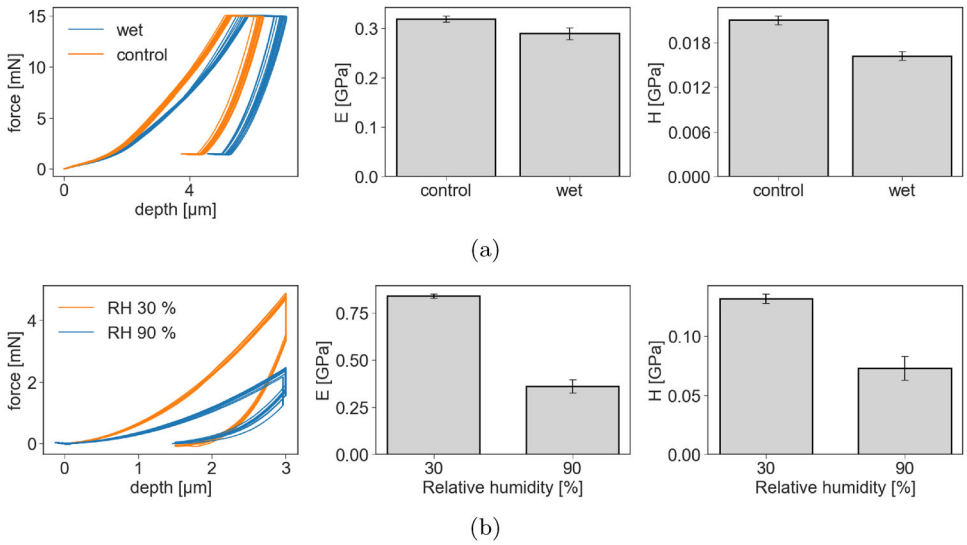

Fig. 7. Nanoindentation force–displacement curves and mechanical properties of Nafion117 at different RH: (a) comparison of control and wet sample using the Nano XP indenter in ambient conditions; maximum load was 15 mN, loading time 10 s, holding time 60 s (strain rate: 0.05 s^{-1}); (b) comparison of a control sample using the Hysitron indenter at different RH: maximal displacement of 3 μm with 10 s loading time and 60 s holding time (strain rate: 0.1 s^{-1}). Error bars the standard deviation of the average value using a minimum of 9 measurements. Young's modulus and hardness were evaluated using the Oliver–Pharr method.[17]

of the slope κ in the plastic regime. Overall, the influence of displacement rate on the elastic and plastic slopes was found to be moderate, as also observed by Lu et al.[31]

Nanoindentation

Figure 5 illustrates the nanoindentation analysis performed on Nafion117 using both the Oliver–Pharr method[17] and the Mokhtari-correction.[14] Unlike the Oliver–Pharr method,[17] which assesses stiffness at a single point during unloading (Fig. 5a), the Mokhtari-correction involves evaluating the stiffness at each time increment along the unloading curve (Fig. 5b), yielding a depth-dependent function of Young's modulus during unloading (Fig. 5c). An inflection point was identified at $P = 40\%P_{max}$ in Fig. 5c, which is consistent with the value determined by tensile testing.

The Mokhtari-correction is based on the observation of stiffness reduction during the unloading of a viscoelastic polymer. This reduction is most prominent at the beginning of the unloading curve, leading to higher values of E, as depicted in Fig. 5c. Mokhtari et al.[14] observed a distinct nonlinear decrease in Young's modulus during their polypropylene (PP) measurements, while Nafion117 exhibited different behavior. The inflection point in Young's modulus, where E values decrease in Fig. 5c, corresponds to the moment when the indenter initiates detachment from the material surface.[14]

Figure 6 summarizes the Young's modulus values determined by the different methods and instruments for the untreated Nafion117 membrane. The comparison includes the elastic modulus determined by tensile testing (in green) and nanoindentation with two instruments (in orange and blue) using the Oliver–Pharr method, the Mokhtari-correction, and the Ngan-correction.

The Oliver–Pharr analysis[17] resulted in Young's modulus values that exceeded the values obtained from tensile tests by a factor of up to 2.5, as also observed in Refs. 14 and 32.

The Ngan-correction[25] yielded a reduction in the elastic modulus compared to the Oliver–Pharr method.[17] This correction relies on exploiting similarities between elasticity and linear viscoelasticity theory.[18] Linear viscoelasticity is a first-order approximation to polymer deformation, and as a linear approximation limited to elastomer-like materials, and is less suited for small-strain thermoplastic behavior. It is worth noting that linear viscoelasticity fails to capture plastic or viscoplastic deformation in glassy polymers when strains approach or exceed the yield strain.[33] Additionally, accurately determining the transition between elastic and plastic deformation during loading in nanoindentation, especially with sharp tips (such as the Berkovich and Vickers tips used in this study), poses challenges. It has been argued that the entire deformation should not be assumed as linear viscoelasticity due to the plastic strain contributions at high loads during indentation.[34] Given the difficulty in distinguishing between elastic and viscoplastic deformation with sharp tips, using spherical and flat-ended tips with advanced dynamic methods is advantageous for determining the limit of linear viscoelasticity.

In addition, the Mokhtari-correction[14] gave modulus values closer to those obtained from the tensile tests. The correction is particularly appropriate for the Nano XP indenter which has a higher resolution in displacement and force measurement compared to the Fischerscope indenter. The Mokhtari-correction overestimated the modulus determined by the Fischerscope compared to the modulus obtained by the tensile test.

Since the Mokhtari-correction evaluated the stiffness at a lower force in the unloading curve, which reduced the number of available data points for the power law fit (Eq. 4) compared to the Oliver–Pharr method, the statistical error increased due to the reduced number of data points when using this method. Furthermore, the Mokhtari-correction was designed for polymers such as PP, which typically has an elastic modulus up to 6–7 times higher than that of the Nafion117 membrane.[35] Consequently, the inflection point (Fig. 5c) is more difficult to identify for the compliant Nafion117 than for the stiff PP, as the signal-to-noise ratio is lower for Nafion117.

The modulus values obtained using the Fischerscope are consistently higher than those obtained using the Nano XP indenter. This difference can be attributed to several factors, such as variations in humidity during measurements, differences in tip geometries, or differences in surface detection. The Fischerscope experiments were conducted in a protective Ar environment with negligible RH ($\sim 0.1\%$), while the Nano XP measurements were conducted under ambient conditions. The difference in RH might have contributed significantly to the differences in modulus values obtained using the two instruments. The observed differences could also be related to the difference in tip geometries. The Nano XP was equipped with a Berkovich tip, a three-sided pyramid, while the Fischerscope used a Vickers tip, a four-sided pyramid. Additionally, accurate surface detection is a challenge in polymer nanoindentation, which we addressed by correcting the surface determined using the Nano XP indenter. Unfortunately, this correction is not possible with the Fischerscope since the data before contact are typically not saved.

To investigate the effect of moisture on the mechanical properties, the Nafion117 membrane was indented at different humidity levels. Figure 7a shows the load–displacement curves as well as the Young's modulus and hardness values for the control and wet samples determined at ambient conditions with the Nano XP indenter. A slight decrease in the mechanical properties is observed in the wet sample compared to the control sample. This change in properties is more significant for hardness than for modulus.

Figure 7b shows the load–displacement curves as well as the Young's modulus and hardness values for the Nafion117 sample determined with the Hysitron indenter at different RH, i.e., at ambient RH $\sim 30\%$ and at elevated RH $\sim 90\%$. A significant decrease in the mechanical properties is observed at elevated RH compared to the mechanical properties at ambient RH, showing a twofold decrease in Young's modulus and hardness with increasing RH.

The difference between the results obtained by the two instruments can be attributed to Schroeder's Paradox,[36] which describes the difference in solvent uptake by a polymer exposed to saturated vapor versus a pure liquid. In addition, there are differences in the swelling mechanisms observed at different humidity levels. At low relative humidity, only a small amount of water is adsorbed, corresponding to the solvation of protons and sulfonate ions. The water in the polymer in this swelling mechanism interacts with the ionic components within the ionomer, helping to overcome the strong tendency of the polymer to exclude water due to its hydrophobic nature and swelling resistance. At RHs $> 70\%$, a greater water uptake occurs, and the absorbed water molecules fill the micro-channels of the ionomer resulting in membrane swelling.[30]

Water generally acts as a plasticizer and reduces the mechanical properties of Nafion117,[22] which is consistent with the results presented in this paper. In addition, excessive water loading has been reported to cause mechanical instability in other membranes, such as anion exchange membranes.[37] Since humidity has an influence on the reported mechanical properties, it is important to control/record the humidity. Otherwise, different humidity levels during membrane storage and during testing could lead to large variations.

CONCLUSION

Based on tensile and nanoindentation experiments of Nafion membranes with different surface treatments, the following conclusions are drawn:

- Young's modulus of Nafion117 was calculated from tensile tests to be 0.2 GPa. The modulus value was not affected by surface treatment or displacement rate.
- The Oliver–Pharr method[17] overestimated Young's modulus compared to the modulus determined by tensile testing and a correction should be applied.
- The Mokhtari-correction[14] reduced the nanoindentation modulus to a value comparable to the tensile test modulus, but with reduced statistical confidence compared to the Oliver–Pharr method[17] for compliant Nafion117.
- The Ngan-correction[25] accounted for the viscous behavior and reduced the modulus compared to the modulus obtained by the Oliver–Pharr method.[17]
- Humidity greatly influences the mechanical properties of the membrane, resulting in a decrease in both Young's modulus and hardness. To ensure accurate testing, it is imperative to

store and test membranes under controlled conditions or to record the relative humidity (RH) at each step.

AUTHOR CONTRIBUTIONS

VY: Conceptualization, Methodology, Investigation, Formal analysis, Data curation, Software, Writing–Original draft preparation, Visualization, NU: Investigation, Resources, Writing–Reviewing and Editing, JB: Investigation, Writing–Reviewing and Editing, FH: Writing–Reviewing and Editing, Supervision, RAE: Supervision, FS: Writing–Reviewing and Editing, Supervision, SB: Data curation, Software, Writing–Reviewing and Editing, Supervision, RS: Writing–Reviewing and Editing, Supervision

FUNDING

Open Access funding enabled and organized by Projekt DEAL.

CONFLICT OF INTEREST

We confirm that we have no financial or other interest in the subject/matter of this work, which may be considered as constituting a real, potential or apparent conflict of interest.

OPEN ACCESS

REFERENCES

1. M.A. Rosen and S. Koohi-Fayegh, *Energy Ecol. Environ.* 1, 10 https://doi.org/10.1007/s40974-016-0005-z (2016).
2. M.B. Satterfield, P.W. Majsztrik, H. Ota, J.B. Benziger, and A.B. Bocarsly, *J. Polym. Sci. B Polym. Phys.* 44, 2327 https://doi.org/10.1002/polb.20857 (2006).
3. P.W. Majsztrik, M.B. Satterfield, A.B. Bocarsly, and J.B. Benziger, *J. Membr. Sci.* 301, 93 https://doi.org/10.1016/j.memsci.2007.06.022 (2007).
4. P.W. Majsztrik, Ph.D. Thesis, Princeton University (2008).
5. Y. Tang, A.M. Karlsson, M.H. Santare, M. Gilbert, S. Cleghorn, and W.B. Johnson, *Mater. Sci. Eng. A* 425, 297 https://doi.org/10.1016/j.msea.2006.03.055 (2006).
6. V. Stanic, *ECS Proc. Vol.* 2004–21, 391 https://doi.org/10.1149/200421.0391PV (2004).
7. R. Sigwadi, M.S. Dhlamini, T. Mokrani, F. Nemavhola, P.F. Nonjola, and P.F. Msomi, *Heliyon* 5, e02240 https://doi.org/10.1016/j.heliyon.2019.e02240 (2019).
8. D.C. Seo, I. Jeon, E.S. Jeong, and J.Y. Jho, *Polymers* 12, 1375 https://doi.org/10.3390/polym12061375 (2020).
9. R. Xia, H. Zhou, R. Wu, and W.P. Wu, *Polymers* 8(9), 344 https://doi.org/10.3390/polym8090344 (2016).
10. R. Xia, H. Zhou, Z. Zhang, R. Wu, and W.P. Wu, *Polym. Eng. Sci.* 58, 2071 https://doi.org/10.1002/pen.24818 (2018).
11. Z. Zhang, C. Tian, Z. Yuan, J. Li, W.P. Wu, and R. Xia, *Mater. Res. Express* 6, 055304 https://doi.org/10.1088/2053-1591/ab008b (2019).
12. L. Gargallo and D. Radic, *Physicochemical Behavior and Supramolecular Organization of Polymers* (Springer Netherlands, Dordrecht, 2009).
13. A.C. Fischer-Cripps, *Nanoindentation Testing* (Springer, New York, 2011), pp21–37.
14. A. Mokhtari, N. Tala-Ighil, and Y.A. Masmoudi, *J. Mater. Eng. Perform.* 31, 2715 https://doi.org/10.1007/s11665-021-06386-9 (2022).
15. M.R. VanLandingham, J.S. Villarrubia, W.F. Guthrie, and G.F. Meyers, *Macromol. Symp.* 167, 15 https://doi.org/10.1002/1521-3900(200103)167:1<15::AID-MASY15>3.0.CO;2-T (2001).
16. D.M. Ebenstein and K.J. Wahl, *J. Colloid Interface Sci.* 298, 652 https://doi.org/10.1016/j.jcis.2005.12.062 (2006).
17. W. Oliver and G. Pharr, *J. Mater. Res.* 7, 1564 https://doi.org/10.1557/JMR.1992.1564 (1992).
18. G. Feng and A.H.W. Ngan, *J. Mater. Res.* 17, 660 https://doi.org/10.1557/JMR.2002.0094 (2002).
19. S.M. Alia, K.S. Reeves, J.S. Baxter, and D.A. Cullen, *J. Electrochem. Soc.* 167, 144512 https://doi.org/10.1149/1945-7111/abc746 (2020).
20. E. Jones, T. Oliphant, and P. Peterson, SciPy: open source scientific tools for Python (2001).
21. E. Hearn, *Mechanics of Materials 1* (Elsevier, Amsterdam, 1997), pp1–26.
22. F. Bauer, S. Denneler, and M. Willert-Porada, *J. Polym. Sci. B Polym. Phys.* 43, 786 https://doi.org/10.1002/polb.20367 (2005).
23. S.F. Parker and S. Shah, *RSC Adv.* 11, 9381 https://doi.org/10.1039/D1RA00791B (2021).
24. B.N. Lucas and W.C. Oliver, *Metall. Mater. Trans. A* 30, 601 https://doi.org/10.1007/s11661-999-0051-7 (1999).
25. A. Ngan, H. Wang, B. Tang, and K. Sze, *Int. J. Solids Struct.* 42, 1831 https://doi.org/10.1016/j.ijsolstr.2004.07.018 (2005).
26. J. Deuschle, Mechanics of soft polymer indentation. https://doi.org/10.18419/OPUS-907 (2008).
27. ...C.R. Harris, K.J. Millman, S.J. Van Der Walt, R. Gommers, P. Virtanen, D. Cournapeau, E. Wieser, J. Taylor, S. Berg, N.J. Smith, R. Kern, M. Picus, S. Hoyer, M.H. Van Kerkwijk, M. Brett, A. Haldane, J.F. Del Río, M. Wiebe, P. Peterson, P. Gérard-Marchant, K. Sheppard, T. Reddy, W. Weckesser, H. Abbasi, C. Gohlke, and T.E. Oliphant, *Nature* 585, 357 https://doi.org/10.1038/s41586-020-2649-2 (2020).
28. P. Paufler, *Cryst. Res. Technol.* 27, 470 https://doi.org/10.1002/crat.2170270407 (1992).
29. J.M. Haudin and B. Monasse, *Handbook of Materials Behavior Models* (Elsevier, Amsterdam, 2001), pp255–264.
30. V. Bharath, J. Millichamp, T. Neville, T. Mason, P. Shearing, R. Brown, G. Manos, and D. Brett, *J. Membr. Sci.* 497, 229 https://doi.org/10.1016/j.memsci.2015.09.027 (2016).
31. Z. Lu, M. Lugo, M.H. Santare, A.M. Karlsson, F.C. Busby, and P. Walsh, *J. Power Sources* 214, 130 https://doi.org/10.1016/j.jpowsour.2012.04.094 (2012).
32. A. Strojny, X. Xia, A. Tsou, and W.W. Gerberich, *J. Adhes. Sci. Technol.* 12, 1299 https://doi.org/10.1163/156856198X00452 (1998).
33. J. Bergström, *Mechanics of Solid Polymers* (Elsevier, Amsterdam, 2015), pp309–351.

34. S. Weyand, Mikromechanische Charakterisierung Multifunktionaler NIPU-Materialien und NIPU-(Nano) Komposite. https://doi.org/10.5445/IR/1000117831 (2020).
35. S.U. Handayani, M. Fahrudin, W. Mangestiyono, and A.F. Hadi Muhamad, *J. Vocat. Stud. Appl. Res.* 3, 1 https://doi.org/10.14710/jvsar.v3i1.10868 (2021).
36. C. Vallieres, D. Winkelmann, D. Roizard, E. Favre, P. Scharfer, and M. Kind, *J. Membr. Sci.* 278, 357 https://doi.org/10.1016/j.memsci.2005.11.020 (2006).
37. M.A. Modestino, D.K. Paul, S. Dishari, S.A. Petrina, F.I. Allen, M.A. Hickner, K. Karan, R.A. Segalman, and A.Z. Weber, *Macromolecules* 46, 867 https://doi.org/10.1021/ma301999a (2013).